# Crystal Growth of $Sr_3NaNbO_6$ and $Sr_3NaTaO_6$: New Photoluminescent Oxides

M. Bharathy, V. A. Rassolov, and H.-C. zur Loye*

*Department of Chemistry and Biochemistry, University of South Carolina, Columbia, South Carolina 29208*

*Received November 5, 2007. Revised Manuscript Received January 11, 2008*

Single crystals of $Sr_3NaNbO_6$ and $Sr_3NaTaO_6$ were grown out of high-temperature $Sr(OH)_2$/NaOH melts contained in silver reaction vessels. Block- and rod-shaped crystals of $Sr_3NaNbO_6$ and $Sr_3NaTaO_6$ were isolated from sealed silver tubes and open crucibles, respectively. The structures were determined by single-crystal X-ray diffraction. Both $Sr_3NaNbO_6$ and $Sr_3NaTaO_6$ crystallize in the trigonal (rhombohedral) system, *R*-3*c* with $a = 9.7853(12)$ Å, $c = 11.606(3)$ Å, $V = 962.4(3)$ Å$^3$, $Z = 6$ ($Sr_3NaNbO_6$), and $a = 9.7867(4)$ Å, $c = 11.6109(7)$ Å, $V = 963.10(8)$ Å$^3$, $Z = 6$, ($Sr_3NaTaO_6$). The oxides are isostructural with the 2H-perovskite related $K_4CdCl_6$ structure type and consist of one-dimensional chains containing face-sharing $NbO_6$ ($TaO_6$) octahedra and $NaO_6$ trigonal prisms. These chains in turn are separated from one another by infinite chains of strontium cations located in a distorted square antiprismatic environment. Interestingly, depending on the exact synthetic conditions, either green or brown crystals with distinct UV–visible spectra were obtained for both $Sr_3NaNbO_6$ and $Sr_3NaTaO_6$. All crystals luminesce at room temperature with violet emissions upon excitation at 250 nm. To better understand the luminescence of these oxides, we performed semiempirical calculations to ascertain the nature of the excited state.

## Introduction

Transition metal oxides with diverse compositions, such as $Sr_3NiPtO_6$,[1] $Sr_3CuIrO_6$,[2] $Ca_{3.1}Cu_{0.9}RuO_6$,[3] $Ca_3Co_2O_6$,[4] $Sr_6Rh_5O_{15}$,[5] and $Ba_{1+x}[(Cu_xRh_{1-x})O_3]$,[6] form in the 2-H-perovskite related structure and have been extensively studied because of their variable compositions and interesting magnetic properties. The structures of the oxides belonging to this family are derived from the stacking of mixed $[A_3O_9]$ and $[A_3A'O_6]$ layers along the *c* axis.[7] Subsequent filling of the interstitial octahedral sites with *B* cations results in a structural formula $A_{3n+3m}A'_nB_{3m+n}O_{9m+6n}$, where *m*/*n* is the ratio between the number of $[A_3O_9]$ and $[A_3A'O_6]$ layers.[7,8] The $m = 0$, $n = 1$ member of this family, $A_3A'BO_6$, crystallizes in the $K_4CdCl_6$ structure type, represented by $Sr_4PtO_6$, the prototypical member of this structural family of oxides.[9] Several compositional analogues of $A_3A'BO_6$ have been synthesized both as single crystals and as polycrystalline powders.[10] A major breakthrough has been the application of molten salt[10] or flux techniques[11] to grow single crystals. Molten alkali carbonates, hydroxide, and chloride fluxes have been employed successfully for the growth of single crystals.[12–15] Over the past decade, we have focused on the preparation of single crystals via high temperature flux growth and carbonate melts.[10,16–18]

The $A_3A'BO_6$ ($A$ = Ca, Sr, Ba; $A'$ = Li, Na) oxides represent a smaller subgroup of this family, limited by the number of metals that can take up the 5+ oxidation state. In this context, $Ca_3NaBO_6$ ($B$ = Ir, Ru),[19] $Sr_3A'RuO_6$ ($A'$ = Li, Na),[20,21] $Sr_3A'IrO_6$ ($A'$ = Li, Na),[22,23] $Ba_3NaBO_6$ ($B$ = Ir, Ru),[24] $Sr_3A'RhO_6$ ($A'$ = Li, Na),[12] $Sr_3A'BiO_6$ ($A'$ = Li, Na),[25]

* To whom correspondence should be addressed. Tel: (803) 777-6916. Fax: (803) 777-8508. E-mail: zurloye@mail.chem.sc.edu.

(1) Nguyen, T. N.; Giaquinta, G. M.; zur Loye, H.-C. *Chem. Mater.* **1994**, *6*, 1642.
(2) Nguyen, T. N.; Lee, P. A.; zur Loye, H.-C. *Science* **1996**, *271*, 489.
(3) Moore, C. A.; Cussen, E. J.; Battle, P. D. *J. Solid State Chem.* **2000**, *153*, 254.
(4) Aasland, S.; Fjellvag, H.; Hauback, B. *Solid State Commun.* **1997**, *101*, 187.
(5) Stitzer, K. E.; El Abed, A.; Darriet, J.; zur Loye, H.-C. *J. Am. Chem. Soc.* **2001**, *123*, 8790.
(6) Zakhour-Nakhl, M.; Claridge, J. B.; Darriet, J.; zur Loye, H.-C. *J. Am. Chem. Soc.* **2000**, *122*, 1618.
(7) Darriet, J.; Subramanian, M. A. *J. Mater. Chem.* **1995**, *5*, 543.
(8) Perez-Mato, J. M.; Zakhour-Nakhl, M.; Weill, F.; Darriet, J. *J. Mater. Chem.* **1999**, *9*, 2795.
(9) Randall, J. J.; Katz, L. *Acta Crystallogr.* **1959**, *12*, 519.
(10) Stitzer, K. E.; Darriet, J.; zur Loye, H.-C. *Curr. Opin. Solid State Mater. Sci.* **2001**, *5*, 535.
(11) Elwell, D.; Scheel, H. J. *Crystal Growth from High-Temperature Solutions*; Academic Press: New York, 1975.
(12) Reisner, B. A.; Stacy, A. M. *J. Am. Chem. Soc.* **1998**, *120*, 9682.
(13) Claridge, J. B.; Layland, R. C.; Henley, W. H.; zur Loye, H.-C. *Z. Anorg. Allg. Chem.* **1998**, *624*, 1951.
(14) Smith, M. D.; Stalick, J. K.; zur Loye, H.-C. *Chem. Mater.* **1999**, *11*, 2984.
(15) Davis, M. J.; Smith, M. D.; zur Loye, H.-C. *Acta Crystallogr., Sect. C* **2001**, *57*, 1234.
(16) Henley, W. H.; Claridge, J. B.; Smallwood, P. L.; zur Loye, H.-C. *J. Cryst. Growth* **1999**, *204*, 122.
(17) zur Loye, H.-C.; Layland, R. C.; Smith, M. D.; Claridge, J. B. *J. Cryst. Growth* **2000**, *211*, 452.
(18) Claridge, J. B.; Layland, R. C.; Henley, W. H.; zur Loye, H.-C. *Chem. Mater.* **1999**, *11*, 1376.
(19) Claridge, J. B.; Layland, R. C.; Adams, R. D.; zur Loye, H.-C. *Z. Anorg. Allg. Chem.* **1997**, *623*, 1131.
(20) Darriet, J.; Grasset, F.; Battle, P. D. *Mater. Res. Bull.* **1997**, *32*, 139.
(21) Frenzen, S.; Muller-Buschbaum, Hk. *Z. Naturforsch.* **1995**, *50b*, 581.
(22) Segal, N.; Vente, J. F.; Bush, T. S.; Battle, P. D. *J. Mater. Chem.* **1996**, *6*, 395.
(23) Frenzen, S.; Muller-Buschbaum, Hk. *Z. Naturforsch.* **1996**, *51b*, 225.
(24) Frenzen, S.; Muller-Buschbaum, Hk. *Z. Naturforsch.* **1996**, *51b*, 1204.

10.1021/cm703157t CCC: $40.75 
Published on Web 03/01/2008

$Ba_3NaBiO_6$,[25] and $Sr_3NaSbO_6$[26] have been synthesized. However, while there exist many examples of $A_3A'BO_6$ oxides containing late transition metals, the only reported oxides of the $A_3A'BO_6$ type containing an early transition metal are $Ba_3NaNbO_6$ and $Ba_3NaTaO_6$.[27] Both of these oxides were synthesized by the solid-state method at 1100 °C and were shown to exhibit photoluminescence at 4.2 K.[28] In our attempts to carry out early transition metal ion substitution on the *B* site in the $A_3A'BO_6$ structure type, we succeeded in growing crystals of $Sr_3NaNbO_6$ and $Sr_3NaTaO_6$ by the molten hydroxide flux method at 700 °C using both sealed silver tubes as well as open silver crucibles. Interestingly, the change in the reaction vessel results in the formation of isostructural materials of different colors. All the oxides show violet emission upon excitation at 250 nm at room temperature. To the best of our knowledge, these are the first examples of oxides containing isolated $NbO_6$ ($TaO_6$) octahedra that exhibit photoluminescence at room temperature.

## Experimental Section

**Materials.** $Nb_2O_5$ (Alfa Aesar, 99.5%), $Ta_2O_5$ (Acros Organics, 99.5%), $Sr(OH)_2$ (Alfa Aesar, 99.99%) and NaOH (Alfa Aesar, 99.5%) were used as received.

**Crystal Growth.** Single crystals of $Sr_3NaNbO_6$ and $Sr_3NaTaO_6$ were grown from a $Sr(OH)_2$/NaOH flux. Green crystals of $Sr_3NaNbO_6$ and $Sr_3NaTaO_6$ were grown in silver tubes. $Nb_2O_5$ (1 mmol), $Ta_2O_5$ (1 mmol), $Sr(OH)_2$ (8 mmol) and NaOH (75 mmol) were loaded in silver tubes that were flame-sealed at one end. The open ends of the filled tubes were then crimped and folded twice before the tubes were placed upright into a programmable furnace. Brown crystals of $Sr_3NaNbO_6$ and $Sr_3NaTaO_6$were grown in silver and alumina crucibles. $Nb_2O_5$ and $Ta_2O_5$ (0.5 mmol), $Sr(OH)_2$ (8 mmol) and NaOH (75 mmol) were placed into silver crucibles and covered loosely with silver lids. The filled silver tubes and crucibles were heated to a reaction temperature of 700 at 600 °C/h. The silver tubes and crucibles were held at 700 °C for 12 h, slowly cooled to 600 °C at 10 °C/h and then furnace cooled to room temperature. The crystals in each case were separated from the flux by dissolving the flux in water and subsequently isolated by vacuum filtration. Phase-pure samples were obtained in case of the green crystals of both $Sr_3NaNbO_6$ and $Sr_3NaTaO_6$.

**Powder X-ray Diffraction.** Powder X-ray diffraction patterns were collected on a Rigaku D/max 2100 powder diffractometer using Cu Kα radiation. Green and brown crystals of $Sr_3NaNbO_6$ and $Sr_3NaTaO_6$, isolated as described above, were crushed and finely ground in an agate mortar. Powder diffraction patterns were collected using these powders. *Le Bail* profile fits were performed using JANA2000[29] to confirm the purity of the powder samples in each case. The unit-cell parameters of $Ba_3NaNbO_6$[27] were used as a starting model for the profile fit.

**Scanning Electron Microscopy.** Scanning electron micrographs of the single crystals of the brown and green forms of $Sr_3NaNbO_6$ and $Sr_3NaTaO_6$ were obtained using a FEI Quanta SEM instrument operated in the low vacuum mode. The crystal shapes and morphologies of both forms of $Sr_3NaNbO_6$ and $Sr_3NaTaO_6$ are shown in Figure 1. Energy-dispersive spectroscopy verified the presence of Sr, Na, and the respective transition element (Nb and Ta) and, within the detection limits of the instrument, confirmed the absence of extraneous elements, such as silver and aluminum.

**Single-Crystal X-ray Diffraction.** Single-crystal data for the green and brown crystals of $Sr_3NaNbO_6$ and $Sr_3NaTaO_6$ were collected on a Bruker SMART APEX CCD based diffractometer with a crystal-to-detector distance of 5.016 cm using monochromated Mo Kα radiation. The data were collected in 4 sets of runs covering a complete sphere of reciprocal space, each set with a different $\varphi$ angles ($\varphi$ = 0, 90, 180, and 0°); each frame covered 0.3° in $\omega$. The data were integrated using SAINTPLUS[30] and an empirical absorption correction was applied in each case. The structures were solved by direct methods with SHELXS97[31] and refined using SHELXL97.[32] Crystallographic data and details of the single crystal data collection of the brown forms of $Sr_3NaNbO_6$ and $Sr_3NaTaO_6$ are given in Table 1. Further details of the crystal structure investigations can be obtained from the Fachinformationszentrum Karlsruhe, 76344 Eggenstein-Leopoldshafen, Germany (fax: (49) 7247-808-666; e-mail: crystdata@fiz-karlsruhe.de) on quoting the depository numbers CSD 418491–418494.

**Optical Properties.** The UV–visible diffuse reflectance spectra of the green and brown forms of $Sr_3NaNbO_6$ and $Sr_3NaTaO_6$ were obtained on a Shimadzu UV/vis NIR scanning spectrophotometer equipped with an integration sphere. The diffuse reflectance spectra were converted to absorbance spectra by the Kubelka–Munk method using the Shimadzu software. Both the green and brown forms of $Sr_3NaNbO_6$ and $Sr_3NaTaO_6$ showed violet emission under a UV hand-held lamp that predominately irradiated at 250 nm. Detailed photoluminescence spectra were recorded on a UV–vis Fluorat-02-Panorama spectrofluorometer at room temperature.

**Calculations.** Semiempirical PM6 calculations were performed using MOPAC2007,[33] with periodic boundary conditions and geometries obtained from the single crystal X-ray diffraction data of $Sr_3NaNbO_6$ and $Sr_3NaTaO_6$.

## Results and Discussion

**Crystal Structures of $Sr_3NaNbO_6$ and $Sr_3NaTaO_6$.** Crystal growth of $Sr_3NaNbO_6$ and $Sr_3NaTaO_6$ was achieved by the reactive hydroxide flux method using a combination of $Sr(OH)_2$, NaOH and the respective transition metal oxide, $M_2O_5$ ($M$ = Nb, Ta). Both $Sr_3NaNbO_6$ and $Sr_3NaTaO_6$ were found to be isostructural with the $K_4CdCl_6$ structure type and crystallize in the trigonal (rhombohedral) system $R\text{-}3c$, with $a$ = 9.7853(12) Å, $c$ = 11.606(3) Å, $V$ = 962.4(3) Å$^3$, $Z$ = 6 and $a$ = 9.7867(4) Å, $c$ = 11.6109(7) Å, $V$ = 963.10(8) Å$^3$, $Z$ = 6, respectively. The atomic positions of the Nb, Ta and Sr atoms were obtained by direct methods. The Na and O atoms were located by subsequent difference Fourier synthesis. All atoms were refined with anisotropic displacement parameters. Since Nb and Sr atoms have similar X-ray scattering factors, bond valence sum calculations were performed to help differentiate between them. The

(25) Carlson, V. A.; Stacy, A. M. *J. Solid State Chem.* **1992**, *96*, 332.
(26) Battle, P. D.; Hartwell, S. J.; Moore, C. A. *Inorg. Chem.* **2001**, *40*, 1716.
(27) Wehrum, G.; Hoppe, R. *Z. Anorg. Allg. Chem.* **1992**, *617*, 45.
(28) Blasse, G.; Dirksen, G. J.; Zhiwu, Pei.; Wehrum, G.; Hoppe, R. *Chem. Phys. Lett.* **1993**, *215*, 363.
(29) Petricek, V.; Ducek, M. *JANA2000 Structure Determination Software Programs*; Institue of Physics,: Praha, Czech Republic, 2000.
(30) *SAINT*, version 6.45a; Bruker AXS Inc.: Madison, WI, 2000.
(31) Sheldrick, G. M. *SHELXS97. Program for Crystal Structure Solution.* University of Gottingen: Gottingen, Germany, 1997.
(32) Sheldrick, G. M. *SHELXL97. Program for Crystal Structure Refinement.* University of Gottingen: Gottingen, Germany, 1997.
(33) James Stewart, J. P. *MOPAC*, version 7.101L; Stewart Computational Chemistry: Colorado Springs, CO, 2007.

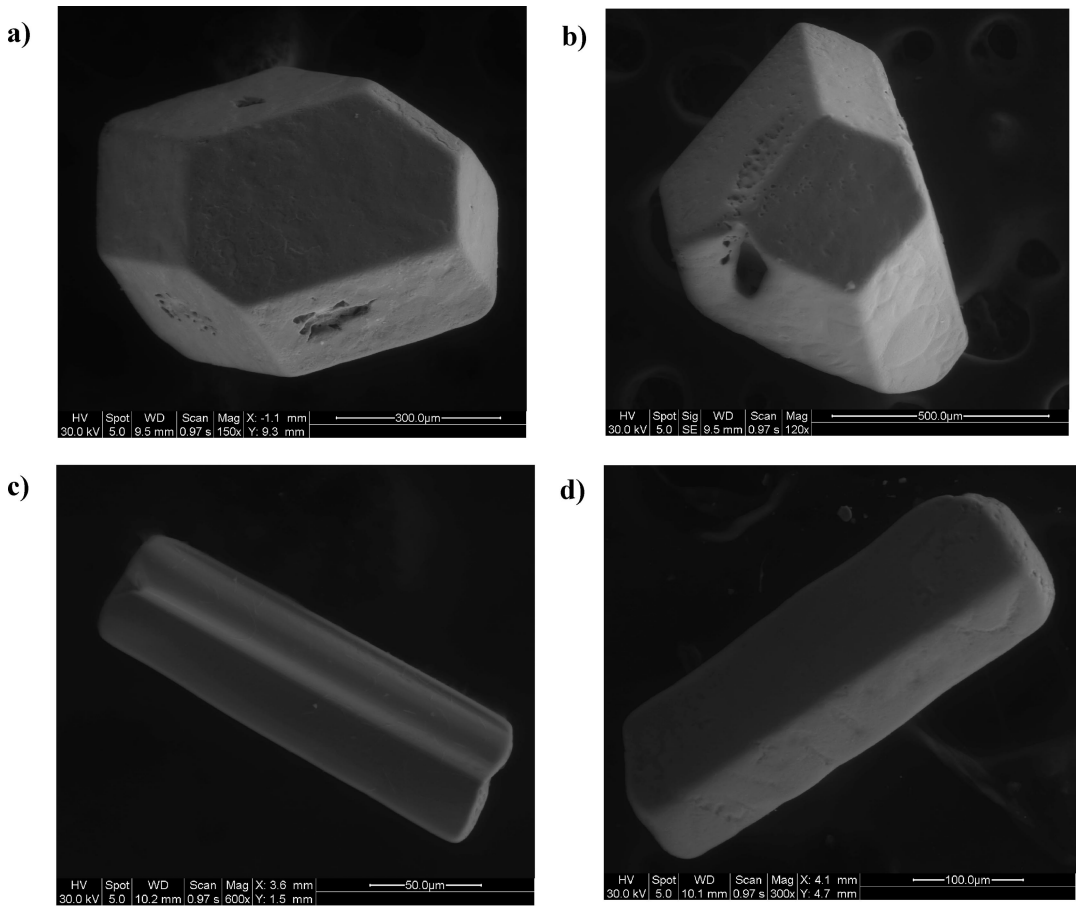


**Figure 1.** SEM pictures of the crystal morphologies of the green (a) $Sr_3NaNbO_6$ and (b) $Sr_3NaTaO_6$ and brown forms of (c) $Sr_3NaNbO_6$ and (d) $Sr_3NaTaO_6$.

**Table 1. Crystallographic Data of $Sr_3NaNbO_6$ and $Sr_3NaTaO_6$**

| | | |
|---|---|---|
| empirical formula | $Sr_3NaNbO_6$ | $Sr_3NaTaO_6$ |
| cryst habit, color | rod, light brown | rod, light brown |
| cryst size ($mm^3$) | $0.2 \times 0.1 \times 0.05$ | $0.3 \times 0.21 \times 0.15$ |
| cryst syst | hexagonal | hexagonal |
| space group | *R*-3*c* | *R*-3*c* |
| cell dimensions (Å/deg) | $a = 9.7853$ (12), $c = 11.606$ (3) | $a = 9.7867$ (4), $c = 11.6109$ (7) |
| $V$ ($Å^3$) | 962.4 (3) | 963.10 (8) |
| fw | 474.76 | 562.80 |
| $D_x$ ($g/cm^3$) | 4.915 | 5.822 |
| $Z$ | 6 | 6 |
| $F$(000) | 1284 | 1476 |
| scan mode | $\omega$ scan | $\omega$ scan |
| $\theta_{max}$ | 35.72 | 35.83 |
| recording reciprocal space | $-15 \le h \le 14$, $-15 \le k \le 15$, $-17 \le l \le 16$ | $-15 \le h \le 13$, $-15 \le k \le 13$, $-16 \le l \le 18$ |
| no. of measured reflns | 3052 | 3226 |
| no. of independent reflns | 469 with $I > 3\sigma(I)$ [$R$(int) = 0.0443] | 497 with $I > 3\sigma(I)$ [$R$(int) = 0.0323] |
| $\mu$ ($mm^{-1}$) | 26.584 | 41.809 |
| refinement | $F^2$ | $F^2$ |
| no. of variables | 19 | 19 |
| $R(F)$ | 0.0264 | 0.0277 |
| $wR(F^2)$ | 0.0726 | 0.067 |
| GOF | 1.185 | 1.38 |
| max/min $\Delta\rho$ (e/$Å^3$) | 0.999/−2.21 | 1.431/−2.38 |

bond valence sums (Table 2) confirm the crystallographic assignments of the atoms and their expected oxidation states in the structure. A view of the crystal structure of $Sr_3NaBO_6$ ($B$ = Nb, Ta) along the $b$ axis is shown in Figure 2. The $A_3A'BO_6$ structure contains infinite chains of face-sharing $A'O_6$ ($A'$ = Na) trigonal prisms and $BO_6$ ($B$ = Nb, Ta) octahedra. These chains are separated from each other by intervening strontium cations that are located in a distorted square antiprismatic coordination environment. The niobium and tantalum containing $BO_6$ octahedra are isolated from one another, being separated from each other by the $NaO_6$ trigonal prisms. An illustration of the isolated (Nb/Ta)$O_6$ octahedra is shown in Figure 3.

The Sr−O distances in the $SrO_8$ square antiprisms range from 2.53 to 2.89 Å, and are slightly shorter than the comparable the Ba-O distances of 2.70–2.98 Å found in the

**Table 2. Selected Bond Distances of the Brown Forms of $Sr_3NaNbO_6$ and $Sr_3NaTaO_6$**

| bond | distance in $Sr_3NaNbO_6$ (Å) | $Sr_3NaTaO_6$ (Å) |
|---|---|---|
| Sr−O(1)[i] × 2 | 2.5378(19) | 2.531(2) |
| Sr−O(1)[ii] × 2 | 2.6157(19) | 2.625(3) |
| Sr−O(1)[iii] × 2 | 2.6265(19) | 2.627(2) |
| Sr−O(1)[iv] × 2 | 2.881(2) | 2.892(3) |
| BVS | 1.908 | 1.898 |
| Na−O(1) × 6 | 2.4031(18) | 2.397(2) |
| BVS | 1.308 | 1.326 |
| Nb/Ta−O(1) × 6 | 2.0020(17) | 2.000(3) |
| BVS | 4.866 | 4.992 |

isostructural $Ba_3NaNbO_6$ and $Ba_3NaTaO_6$.[27] This difference is consistent with the larger size of $Ba^{2+}$ compared to $Sr^{2+}$. The Sr−O bond distances in $Sr_3NaNbO_6$ and $Sr_3NaTaO_6$ are similar to those found in the analogous ruthenate $Sr_3NaRuO_6$ (2.57−2.75 Å).[21] The Na−O bond distances of ∼2.40 Å and the Nb−O and Ta−O distances of ∼2.0 Å in $Sr_3NaNbO_6$ and $Sr_3NaTaO_6$ are in good agreement with interatomic distances found in analogous oxides.[19,26,27]

**Crystal Morphologies and Color.** The reactions were initially carried out in sealed silver tubes and the thus obtained single crystals were hexagonal in shape (images a and b in Figure 1) and pale green in color. The reactions were repeated in covered silver crucibles where, surprisingly, the crystals grown in the crucible were rod shaped (images c and d in Figure 1) and brown in color. To eliminate the possibility of silver contamination, the reactions were also carried out in alumina crucibles. The resultant crystals also were brown rods, suggesting that the color is not due to crucible material impurities, but potentially due to differences in the types of crystal defects (color centers, Frenkel or Schottky defects) present in the crystals. As the crystal morphology varies as a function of the reaction vessels used during the synthesis, it is possible that the growth morphologies influence the types and concentrations of crystal defects. To rule out any unexpected impurities or variation in bulk composition, several crystals of each color and composition were analyzed using a EDS 4 point analysis. No extraneous impurities were detected and all compositions corresponded to $Sr_3NaNbO_6$ or $Sr_3NaTaO_6$.

To investigate the role of defects in the optical behavior, we heated powdered single crystals of $Sr_3NaNbO_6$ and $Sr_3NaTaO_6$ to various temperatures, up to 900 °C, to check if the defects could be annealed out of the structure. While the color did disappear, additional diffraction lines appeared in the powder X-ray diffraction pattern and the structure changes entirely from $A_3A'BO_6$ to the $Ba_3SrNb_2O_9$[34] type by 900 °C. The isostructural $Ba_3NaNbO_6$ and $Ba_3NaTaO_6$ phases, which were synthesized from the respective alkali and alkaline earth carbonates by the solid-state method, are reported to be white in color.[27] Hence we attempted the syntheses of $Sr_3NaNbO_6$ and $Sr_3NaTaO_6$ via the solid state method used for $Ba_3NaNbO_6$ and $Ba_3NaTaO_6$, starting with $SrCO_3$, $Na_2CO_3$, and the respective transition metal oxides in alumina boats. We were unable to obtain the desired product and instead obtained a product that appears to be related to the $Ba_3SrNb_2O_9$ structure.[34] This suggests that the formation of $Sr_3NaNbO_6$ and $Sr_3NaTaO_6$ can be achieved only at low temperatures, such as in the flux environment at 700 °C, or perhaps by some as of yet unknown precursor route.

**UV–Visible Spectra and Photoluminescence.** The diffuse reflectance UV–visible absorbance spectra of $Sr_3NaNbO_6$ and $Sr_3NaTaO_6$ are shown in Figure 4. The measurements were made using powder samples consisting of ground single crystals. The absorption edges in case of both the green and brown forms of $Sr_3NaNbO_6$ and $Sr_3NaTaO_6$ are around 280 nm. There is an additional absorption peak at ∼350 nm in the case of the green forms, and at ∼450 nm in the case of the brown crystals. These additional peaks are consistent with the observed colors of the powders. When illuminated by a hand-held UV lamp (∼250 nm) both the green and brown forms of $Sr_3NaNbO_6$ and $Sr_3NaTaO_6$ exhibit blue/violet colored emission. Figure 5 shows the colors of powdered sample of the brown rods of $Sr_3NaTaO_6$ in daylight (Figure 5a) and under UV illumination (Figure 5b).

The excitation and emission spectra of the brown and green forms of $Sr_3NaNbO_6$ and $Sr_3NaTaO_6$ at 300 K are shown in Figure 6. Using an excitation wavelength of 240 nm, emission spectra with peaks centered at ∼435 nm were observed for the brown and green forms of $Sr_3NaTaO_6$, (Figure 6). The analogous data for the niobates using an excitation wavelength of 278 nm are shown in the inset to Figure 6, with emission peaks at ∼425 nm. The luminescence of the tantalate sample is noticeably stronger than the niobate and, in the latter case, the emission of the green phase is barely measurable. The observation of luminescence in these samples is not entirely unexpected, since the barium analogues, $Ba_3NaNbO_6$ and $Ba_3NaTaO_6$ exhibit strong luminescence at 4.2 K which, however, is quenched at room temperature.[28]

Luminescence of highly charged transition metal ion complexes such as titanates, niobates, tantalates, tungstates and molybdates has been studied for decades.[35–37] In these compounds, typically, the emission was proposed to result from a triplet-singlet transition,[38] which was experimentally verified by Barendswaard *et al*.[39] There are other causes for luminescence and factors such as anion deficiencies and cation disorder can also give rise to luminescence.[40] Charge-transfer vibronic excitons may also play an important role in the luminescence mechanism.[41–43] Semiempirical INDO calculations[43] estimate that the energy of stabilization of excited states due to lattice distortion caused by optical excitation is on the order of 2.0–2.5 eV, yielding excitons with calculated absorption energies close to experimentally observed values. This suggests the viability of a semiempirical approach to understanding the nature of the excited

(34) Zandbergen, H. W.; Ijdo, D. J. W. *Acta Crystallogr., Sect. C* **1983**, *39*, 829.
(35) Blasse, G. *Prog. Solid State Chem.* **1988**, *18*, 79.
(36) Chandrasekhar, B. K.; White, W. B. *Mater. Res. Bull.* **1990**, *25*, 1513.
(37) Bouma, B.; Blasse, G. *J. Phys. Chem. Solids.* **1995**, *56*, 261.
(38) Blasse, G. *Chem. Phys. Lett.* **1979**, *63*, 441.
(39) Barendswaard, W.; Van Tol, J.; Van der Waals, J. H. *Chem. Phys. Lett.* **1985**, *121*, 361.
(40) Blasse, G. *Struct. Bonding* **1980**, *42*, 1.
(41) Vikhnin, V. S.; Eglitis, R. I.; Kapphan, S. E.; Borstel, G.; Kotomin, E. A.; *Phys. Rev. B.* **2002**, *65*, 104304–1.
(42) Vikhnin, V. S. *Solid State Commun.* **2003**, *127*, 283.
(43) Eglitis, R. I.; Kotomin, E. A.; Borstel, G.; Kapphan, S. E.; Vikhnin, V. S. *Comput. Mater. Sci.* **2003**, *27*, 81.

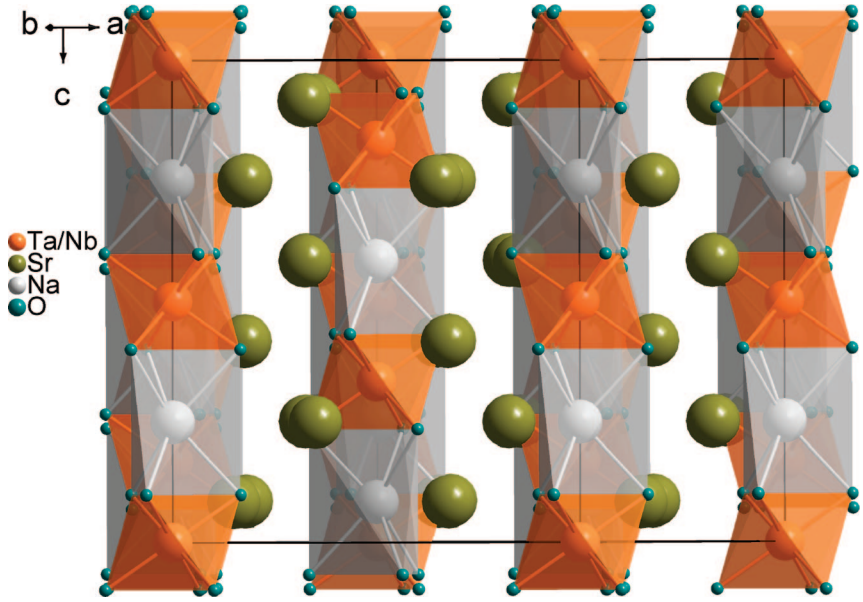


**Figure 2.** Crystal Structure of $Sr_3NaBO_6$ ($B$ = Nb, Ta) along the $b$ axis.

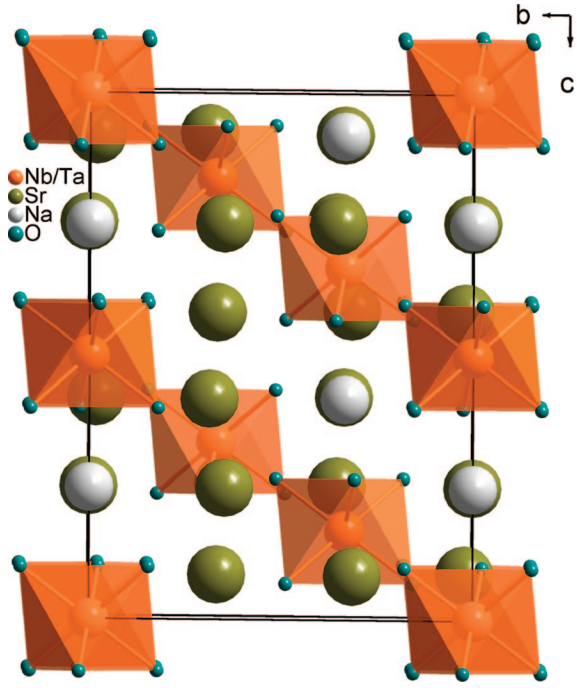


**Figure 3.** Illustration of the isolated $(Nb/Ta)O_6$ octahedra in the $A_3A'BO_6$ structure.

states in perovskites. Delocalization of the excited state is yet another factor that affects luminescence, for example in $LiNbO_3$, $NaNbO_3$ and $KNbO_3$.[44] Structures that exhibit three-dimensional coupling of the $d^0$ metal ion polyhedra through corner sharing and/or edge sharing ($CdNb_2O_6$ and $CaTa_2O_6$) show luminescence owing to delocalization of the excited state.[40] On the other hand, scheelites such as $CaMoO_4$,[36] consisting of isolated $MoO_4$ tetrahedra, have also been observed to exhibit luminescence. The $(Nb/Ta)O_6$ octahedra are isolated in $Sr_3NaNbO_6$ and $Sr_3NaTaO_6$, hence semiempirical calculations were performed to ascertain the nature

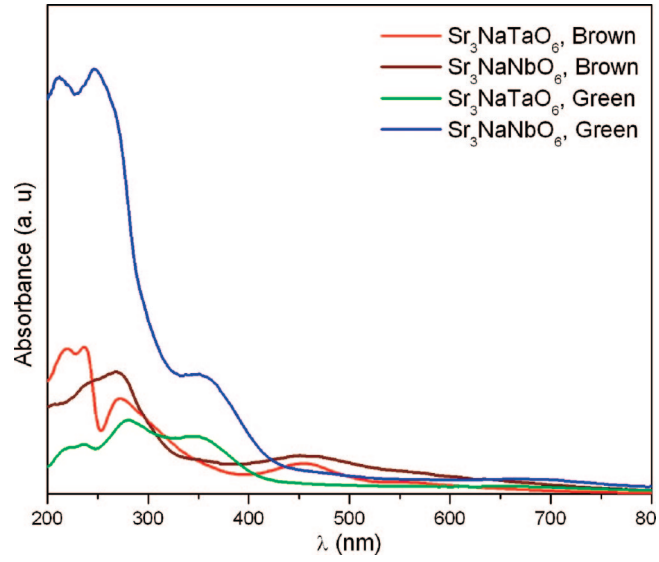


**Figure 4.** UV–visible absorbance spectra of the brown and green forms of $Sr_3NaNbO_6$ and $Sr_3NaTaO_6$.

of the excited state. For these compositions, the HOMO is localized on oxygen 2p states, and the LUMO is shared between the s-orbital of the transition metal (Nb or Ta), and the s-orbital of strontium. The PM6 model gives HOMO–LUMO gaps of about 7 eV for the niobate compounds, and 6 eV for the tantalate compounds. The observed band gaps calculated from UV–visible spectra are in the range 4.39–4.41 eV. It is well-known that orbital energy differences strongly overestimate actual excitation energies, and either Configuration Interaction or time dependent treatment are needed to model the energetics of the electronic excitations. Lattice distortions may also reduce the excitation energies significantly.[41,43] Nevertheless, the orbital energies provide a useful qualitative description. In our calculations the energy gap between the LUMO and the LUMO+1 is about 0.8 eV, which is much larger than energy gaps between other virtual (0.0 to 0.15 eV) or occupied orbitals. This suggests that

(44) Wiegel, M.; Emond, M. H. J.; Stobbe, E. R.; Blasse, G. *J. Phys. Chem. Solids* **1994**, *55*, 773.

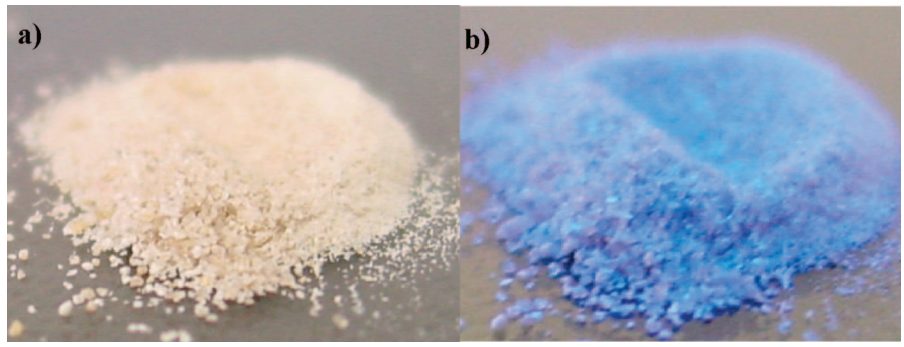


**Figure 5.** Powdered brown crystals of $Sr_3NaTaO_6$ (a) before and (b) after illumination at 250 nm.

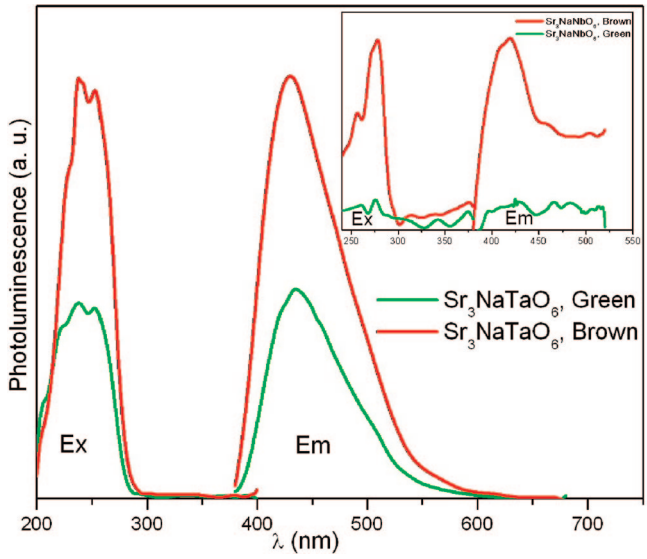


**Figure 6.** Photoluminescence spectra of the (a) green and (b) brown forms of $Sr_3NaNbO_6$ and $Sr_3NaTaO_6$.

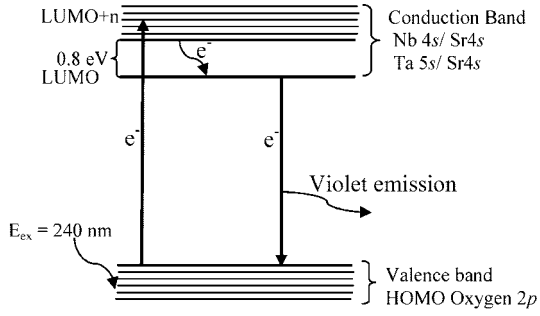


**Figure 7.** Simplified illustration of the likely process of photoluminescence in $Sr_3NaNbO_6$ and $Sr_3NaTaO_6$.

optically excited electrons are localized at the LUMO and do not easily migrate to nonradiative quenching sites.

A simplified illustration of the likely process of photoluminescence in $Sr_3NaNbO_6$ and $Sr_3NaTaO_6$ is shown in Figure 7. Upon an excitation wavelength of 250 nm, an electron is promoted from the valence band or HOMO (comprising of O 2p orbitals) to the conduction band or LUMO. The separation of energy states in the conduction band being higher in energy, (0.8 eV), there is a nonradiative transfer from the LUMO+1 energy state to an intermediate low lying LUMO state which consists of Sr 4*s* and Nb 4*s*orbitals in $Sr_3NaNbO_6$ and Sr 4s and Ta 5s orbitals in $Sr_3NaTaO_6$. A radiative transfer from this intermediate state to the valence band gives rise to violet emission.

The shared population of the LUMO on the transition metal and the strontium cation points to the importance of the interaction between the transition metal and the strontium cation in the luminescence of these compounds. We have attempted to use DFT with local density approximation (LDA) to verify the band structure, but the calculation proved to be beyond our computational capabilities due to the large unit cell size.

We hypothesize that the color observed in these $d^0$ transition metal containing oxides, $Sr_3NaNbO_6$ and $Sr_3NaTaO_6$, is due to a combined effect of the presence of optically active defects and luminescence at room temperature. It is possible that the growth of different morphologies and color of the same material under different reaction vessels implies a variation in the concentration of the defects.

## Conclusion

Single crystals of early transition metal analogues of the $A_3A'BO_6$ structural type, $Sr_3NaNbO_6$ and $Sr_3NaTaO_6$, were grown out of molten hydroxide fluxes. The growth process influenced the crystal color, where crystal growth reactions carried out in sealed silver tubes and silver crucibles resulted in green hexagonal shaped crystals and brown rod-shaped crystals, respectively. The green and the brown crystals have the same crystal structure, but differ in their optical properties. The color variations are attributed to a combined effect of the differences in crystal defects and morphologies owing to different crystal growth processes occurring in different vessels. Both $Sr_3NaNbO_6$ and $Sr_3NaTaO_6$were found to luminescence at room temperature. The photoluminescence at room temperature is ascribed to be due to mixing of the s orbitals of the transition metal and the strontium cation.

**Acknowledgment.** Financial support from the National Science Foundation through Grant DMR 0450103 is gratefully acknowledged. We thank Dr. Sangmoon Park, University of South Carolina, and Prof. Shiou-Jyh Hwu, Clemson University, for access to their fluorescence and UV–visible spectrophotometers, respectively.

CM703157T